TU Delft

Delft University of Technology

Exploring water and ion transport process at silicone/copper interfaces using in-situ electrochemical and Kelvin probe approaches

Munirathinam, Bala; van Dam, Joost; Herrmann, Annemarie; van Driel, Willem; De Buyl, F.; Erich, S. J.F.; van der Ven, L.G.J.; Adan, O. C.G.; Mol, Arjan

DOI
10.1016/j.jmst.2019.07.044

Publication date
2021

Document Version
Final published version

Published in
Journal of Materials Science & Technology: an international journal in the field of materials science

Citation (APA)
Munirathinam, B., van Dam, J., Herrmann, A., van Driel, W., De Buyl, F., Erich, S. J. F., van der Ven, L. G. J., Adan, O. C. G., & Mol, A. (2021). Exploring water and ion transport process at silicone/copper interfaces using in-situ electrochemical and Kelvin probe approaches. *Journal of Materials Science & Technology: an international journal in the field of materials science*, *64*, 203-213. https://doi.org/10.1016/j.jmst.2019.07.044

Important note
To cite this publication, please use the final published version (if applicable).
Please check the document version above.

Copyright
Other than for strictly personal use, it is not permitted to download, forward or distribute the text or part of it, without the consent of the author(s) and/or copyright holder(s), unless the work is under an open content license such as Creative Commons.

Takedown policy
Please contact us and provide details if you believe this document breaches copyrights.
We will remove access to the work immediately and investigate your claim.

This work is downloaded from Delft University of Technology.
For technical reasons the number of authors shown on this cover page is limited to a maximum of 10.

Green Open Access added to TU Delft Institutional Repository

'You share, we take care!' - Taverne project

https://www.openaccess.nl/en/you-share-we-take-care

Otherwise as indicated in the copyright section: the publisher is the copyright holder of this work and the author uses the Dutch legislation to make this work public.

Journal of Materials Science & Technology 64 (2021) 203–213

Contents lists available at ScienceDirect

Journal of Materials Science & Technology

journal homepage: www.jmst.org

Research Article

Exploring water and ion transport process at silicone/copper interfaces using *in-situ* electrochemical and Kelvin probe approaches

B. Munirathinam[a,*], J.P.B. van Dam[a], A. Herrmann[b], W.D. van Driel[c,d], F. De Buyl[e], S.J.F. Erich[b], L.G.J. van der Ven[b], O.C.G. Adan[b], J.M.C. Mol[a,*]

[a] Delft University of Technology, Department of Materials Science and Engineering Department, Delft, The Netherlands
[b] Eindhoven University of Technology, Department of Applied Physics, Eindhoven, The Netherlands
[c] Signify, High Tech Campus, Eindhoven, The Netherlands
[d] Delft University of Technology, Electronic Components, Technology and Materials, Faculty of Electrical Engineering, Delft, The Netherlands
[e] Dow Silicones Belgium s.p.r.l., Belgium

ARTICLE INFO

Article history:
Received 24 April 2019
Received in revised form 21 June 2019
Accepted 1 July 2019
Available online 19 September 2019

Keywords:
Silicone
Impedance
Water transport
Scanning Kelvin probe
Delamination

ABSTRACT

In general, packaging materials which encapsulate light emitting diodes (LEDs) and microelectronic devices offer barrier protection against several environmental hazards such as water and ionic contaminants. However, these encapsulants may provide pathways for water and ionic contaminants to reach the metal/polymer interfaces and provoke local corrosion of electronics, which is a major reliability concern for polymer encapsulated LEDs and microelectronics. As the water and corrosive constituents play a crucial role in their reliability, water uptake kinetics, interfacial ion transport and delamination behaviour of silicone coated copper model system, mimicking a typical microelectronics packaging system, is explored in the present work. Electrochemical impedance spectroscopy (EIS) integrated with attenuated total reflection Fourier transform infrared (ATR-FTIR) spectroscopy studies revealed that water diffusion inside the silicone network is Fickian in nature and the evolution of the observed time constants are related to the diffusion and interfacial reactions. A decrease of impedance magnitude with time was observed in EIS measurements concurrently with water absorption bands shifting towards lower wavenumber in ATR-FTIR measurements, implying the growth of strong hydrogen bonding between water molecules and the silicone network. The estimated diffusion constant of water using the capacitance method was in the order of 7×10^{-12} m^2 s^{-1} and the water absorption volume fraction was in the range of 0% to 0.30%. Scanning Kelvin probe studies elucidated the ion transport process occurring at the silicone/copper interface in a humid atmosphere. The interfacial ion transport process is controlled by the interfacial electrochemical reactions at the cathodic delamination front and the estimated average delamination rate is 0.43 mm $h^{-1/2}$. This work demonstrates that exploring ion and water transport in the silicone coating and along the silicone/copper interface is of pivotal importance as part of a detailed reliability assessment of the polymer encapsulated LEDs and microelectronics.

© 2020 Published by Elsevier Ltd on behalf of The editorial office of Journal of Materials Science & Technology.

1. Introduction

Several environmental service conditions may cause early failure of microelectronics and light emitting diode (LED) devices. Amongst these conditions, corrosion is a key degradation mode as it accounts for approx. 20% of the total failure cases of electronic components [1,2]. Besides, while the demand for miniaturization opens the potential to enhance the performance of these devices, their reliability remains a primary concern as moisture and corrosive contaminants (e.g. oxidants and halogens compounds like chloride, sulphate, bromide) can migrate or diffuse through encapsulant altering the electronic characteristics or decreasing the time to device failure by forming local electrochemical cells.

Generally, these microelectronics and LEDs are encapsulated by polymers which offer barrier protection often regarded as an efficient corrosion protection to them against several environmental hazards. However, these encapsulating polymers are typically slightly hydrophilic in nature and inherently absorb moisture from the humid atmosphere. The corrosive contaminants that emanate

* Corresponding authors.
E-mail addresses: blkrish88@gmail.com (B. Munirathinam), J.M.C.Mol@tudelft.nl (J.M.C. Mol).

https://doi.org/10.1016/j.jmst.2019.07.044
1005-0302/© 2020 Published by Elsevier Ltd on behalf of The editorial office of Journal of Materials Science & Technology.

during fabrication and during the component's service life can combine with water molecules, enhancing mobility of these ions. Upon diffusion through the polymer, the contaminants will reach the packaging/metallic circuitry interface and initiate an interfacial corrosion process. Reports devoted to the basic understanding of the transport phenomena involved are limited [3–7]. Two main transport pathways are identified in the microelectronics and LED packaging systems. In the first type of transport pathways, the ionic species abetted by moisture diffuse through the polymer reaching the interface (regarded as bulk transport), providing necessary conditions for local corrosion. The second mode of transport occurs during lead forming when some delamination may occur between the lead frame and polymer at the location where the leads enter the packaging body. This separation facilitates corrosive ions (e.g. chlorides) to migrate along the bond wires (regarded as interfacial transport) made of Al, Au or Cu, towards the chip, i.e. the exposed metallic bond pads causing corrosion and wire bond lift-off [5].

As the water uptake in polymers is a root cause for the initiation of the corrosion process, researchers worldwide investigated water transport behaviour using electrochemical impedance spectroscopy (EIS), gravimetry, infrared spectroscopy, differential scanning calorimetry, dynamic vapour absorption, finite element analysis and molecular dynamics study [7–12]. Studies have shown that the water and ions penetrate through micropores and free volume of the polymer coatings and surface inhomogeneities or inherent defects may influence their ionic conduction [13,14]. The quantity of water uptake using gravimetric measurements is widely explored, and it is a reliable and a reference method for free standing polymer films [15,16]. Conversely, in some cases it was found to be inadequate due to leaching of organic fragments from the coatings [17,18]. Moreover, its incapability to sense the electrochemical reactions occurring at the metal/film interface has limited its applications.

The EIS is a valuable continuous monitoring technique as it not only determines the barrier film dielectric properties but also probes the reaction occurring at the metal/coating interface upon exposure to a corrosive environment. Early reports on the analysis of EIS data for polymer coated system for innumerable applications proved that its sensitivity to diffusion process has made it a versatile tool for degradation studies [19–22]. Besides, attempts were made to evaluate the water uptake of the protective coatings employed in microelectronic packaging devices. For instance, Belluci [23] elucidated the environmental degradation of a polyimide/aluminium packaging system at different chloride concentrations and deduced that the mode of water uptake is notably affected by the salt concentration, thereby governing the lifetime of the packaging system. According to Madani *et al.* [24], the water uptake in an epoxy/gold system introduces a change in the dielectric properties characterized by appreciable changes in the high frequency range of impedance spectra after 100 h of exposure. This variation was ascribed to the penetration of water and ions facilitating conducting pathways to degrade the epoxy/gold interface. Furthermore, the study focussed principally on the moisture and ionic contaminant uptake using EIS and did not provide further details on the changes in interfacial chemistry as a function of time. A real-time evaluation of moisture induced damage in commercial off-the-shelf devices in plastic-encapsulated microcircuit at the chip level conducted by Pollock *et al.* [25] by EIS measurements revealed that the corrosion of the devices initiates and accelerates as the protective properties of the encapsulant degrades with time. The authors suggested that failure begins by weakening of the interfacial bonds between encapsulant and substrate; however, molecular bonding information is not reported to substantiate their analysis. Recently, increasing efforts have been made to simultaneously investigate the transport of water or any corrosive species at polymer/metal interfaces and the electrochemical reactions using combined *in-situ* attenuated total reflectance Fourier transform infrared spectroscopy (ATR-FTIR) integrated with EIS analysis. Most of these efforts have been devoted to understand the water uptake kinetics, bonding information, mechanism of wetadhesion process occurring at the interface that are encountered in various applications [26–30]. At the same time, no comprehensive systematic studies concerning the interfacial kinetics using the method combined ATR-FTIR and EIS for the interfaces typically used in microelectronics and light emitting diode (LED) packaging systems have been reported, yet.

Another serious issue in the packaging industry is the delamination at polymer/metal interfaces. Several reports addressed the interfacial delamination behaviour encountered in epoxy moulding compound (EMC)/lead frame and EMC/paddle interfaces [31,32]. Silicones are one such encapsulant material in high power LED devices which have received great consideration over epoxy resin in recent decades owing to their outstanding properties like good thermal stability, higher luminous efficiency, better transparency, good barrier properties and higher refractive index [33,34]. On the other hand, it has been proved by Shuto *et al.* [35] that the moisture resistance of silicone is inferior than that of epoxy resin. On account of the low intermolecular interactions in the silicone network, their free volume is higher than hydrocarbons facilitating higher permeability to oxygen and water. To surmount this issue, functional groups like methyl are replaced by part of the phenyl group along the siloxane chains and at the siloxane [36]. The addition of a significant percentage of phenyl groups along the siloxane chain and in the structure of siloxane resins (containing silicon substituent T ($RSiO_{3/2}$) and Q ($SiO_{4/2}$) units) is sufficient to reduce the crystallization, thereby promoting the silicone to remain flexible even at lower temperature. These phenyl group not only offers better resistance to moisture but also improves the refractive index. Besides, their durability also relies on the interfacial strength of the leadframe LED packages. For example, Wang *et al.* [37] performed shearing tests to assess the interfacial strength of typical interfaces found in LED packaging involving silicone encapsulant with copper, ceramic and silicon substrates. Although the results showed that interfacial strength of silicone on copper is higher, authors claim that the strengths of these three interfaces are relatively low, as a consequence, the delamination of these interfaces may become a primary concern for LED packaging. The interfacial adhesion strength between the silicone encapsulant and the side wall of the LED lead-frame cup using customized pin-push test was evaluated by Zhong *et al.* [38] and the normal and shear stress distribution along the concerned interfaces was obtained. Furthermore, Suzuki *et al.* [39] proved that the silicone material acts as diebond adhesive to reduce the thermal mismatch between the silicon die and the copper lead-frame. They also pointed out that ionic contaminants from the die bond adhesive deteriorates its moisture resistance. Based on the aforementioned findings, to understand the interfacial delamination as well as the water transport kinetics is of primary importance in microelectronics and LED packaging system. Generally, in encapsulant microelectronics devices, the interfacial delamination is driven by the transport of corrosive constituents combined with the moisture. The ion mobility along the buried metal/polymer interfaces can be monitored using Scanning Kelvin probe (SKP) by measuring its Volta potential under humid atmosphere. The transport of anions or cations beneath the polymer coating and the oxide surface properties govern their delamination rate. Several previous reports revealed that the delamination process can either be governed by cathodic delamination or anodic undermining depending on the system and condition studied [30,40–45]. However, comprehensive analysis on the delamination kinetics occurring at the polymer encapsulated metallic electronic devices is still lacking, and it is imperative to explore the delamination behaviour of microelectronic and LED

packages under corrosive environmental conditions. Furthermore, there is no systematic report concerning the ion transport phenomena occurring along the interfaces of buried encapsulant materials in microelectronic devices investigated using SKP measurements. Hence, it is of pivotal importance to explore the moisture diffusion and the delamination kinetics as part of a detailed reliability assessment of the silicone encapsulated LEDs and microelectronics.

As the corrosive constituents play a crucial role in package reliability, the influence of corrosive environment as a function of time on the ion transport, delamination and water transport behaviour of the silicone coated copper model system was explored in the current work. An attempt was made to elucidate the water and ion transport mechanisms at different transport pathways encountered in encapsulated microelectronic devices.

2. Experimental

2.1. Sample preparation

Substrate material employed in this work is a commercially available lead frame copper alloy (grade: C51900; nominal composition: Sn - 4.80 at.%, P 0.85 at.%, Cu-rest) sheet supplied by Salomon's Metals, Netherlands. Copper alloy (20 mm × 20 mm × 5 mm) was ground with #1200 SiC grit emery paper, and then it was cleaned with acetone followed by ethanol for 15 min in an ultrasonic bath to get rid of organic impurities on the surface. A commercially available optical grade silicone resins (OE-6650, Part A &B 1:3 ratio; supplied by Dow Corning*) with a high refractive index of 1.54 were used. In contrast to low refractive index silicones, which are made up of pure poly-dimethyl-siloxane (PDMS), this resin contains a higher amount of phenyl-siloxane, which increase the refractive index of the silicone (1.41 in pure PDMS vs. 1.55 in poly-methyl-phenyl siloxane polymer) [7,36]. Now, a thin layer of silicone resin (40 μm) was manually casted on the substrate using bar coater and cured at 150 °C for 2 h. Another set of copper alloy (C581) sheet is used as deposition target and deposited on a ZnSe internal reflection element (IRE) crystal (and on glass substrate to characterize the surface of metallic film) using high vacuum evaporating system in order to mimic similar chemical composition of the metallic substrate on the crystal. The film thickness obtained was 20 ± 5 nm. Subsequently, the silicone coating was applied on by following the aforementioned procedure carried out for the coper alloy sheet.

2.2. Surface characterization

X-ray diffraction (XRD) measurements (Bruker D8 Advance diffractometer) were carried out using an incident Cu Kα radiation (λ =1.54 Å), tube voltage 45 kV at a step size of 0.030° with counting time per step as 1.10 s. Surface morphology of the developed coating was examined using scanning electron microscope (SEM FEI Quanta FEG 400). Energy-dispersive X-ray spectroscopy (EDX) fitted to SEM chamber was used to analyze the composition of the samples.

2.3. Combined ATR-FTIR and electrochemical measurements

ATR-FTIR in Kretschmann geometry configuration integrated with a potentiostat (Thermo Nicolet Nexus FTIR and Solartron FRA 1278A potentiostat) is employed to measure both electrochemical behaviour and transport of infrared active species at the interface between deposited copper film and silicone coating using Zn Se IRE crystal. The measurements were carried out with an incident beam angle of 80° at a resolution of 4 cm^{-1} and 1000 scans per spectrum. The background spectra were recorded initially on the dry sample and the spectra were obtained in the spectral region of 4500 - 600 cm^{-1}. All the spectra are collected in absorbance format, -log (R/R_o), where R and R_o are the reflectance from sample and background, respectively. A conventional three-electrode configuration was used for the tests. A saturated silver/silver chloride was used as the reference electrode, graphite rod as counter electrode and coated specimen as the working electrode. EIS measurements were carried out by sweeping the frequency of the AC perturbation signal from 0.1 to 10 mHz. The amplitude of the AC excitation voltage was 10 mV.

2.4. SKP measurements

Mechanically polished copper alloy sheet (30 mm × 10 mm) is employed as a substrate for SKP (SKP5050, KP Technology) measurements. A part of the specimen (30 mm × 10 mm) is covered with a teflon tape and then the whole area of specimen is coated with silicone. After curing, part of the coating is carefully lifted off from the teflon tape and then the tape is removed from the surface. In this manner, a sharp artificial defect (boundary between coated and uncoated area) is created and an electrolyte reservoir is created by casting resin using a glue gun at the edges of the uncoated region. Measurements were carried out at high relative humidity (RH) of 93% with different exposure time. The reference electrode used was a vibrating stainless steel probe with a diameter of 50 μm at the tip. The probe was set to vibrate at a 62 Hz frequency and the lateral resolution of the probe was in the range of 50 μm. The measured electrode potentials are in reference to the standard hydrogen electrode (SHE) after calibration against $Cu/CuSO_4$ [46]. Delamination front is marked as the boundary of the galvanic element and the position is defined accordingly in the present work using the procedure followed in earlier work [47].

3. Results and discussion

3.1. Crystallinity and functional group analysis

To understand the crystallographic features of the as-received Cu alloy and the deposited metallic film on Zn Se IRE crystal surface, XRD measurements were performed as these features will profoundly influence their electrochemical behaviour. Fig. 1(a) shows the recorded X-ray diffractograms of the samples and the observed peaks correspond only to the diffracted planes of Cu (all matched well with JCPDS No. 04-0836). The diffraction pattern of asreceived Cu alloy reveals that the crystallographic planes of polycrystalline copper are oriented in a random direction and no preferential growth is observed. In contrast, a highly textured close packed (111) plane crystallizes after deposition on the IRE crystal exhibiting an orientation similar to a single crystal. Conceptually, atoms are strongly bonded to each other in close packed planes thereby offering high resistance to dissolution [48]. In addition, (111) textured copper exhibited substantial resistance to electromigration of metal interconnects for high current density applications [49]. The deposited film thickness was less than 50 nm, so the baseline of the data was not flat due to a strong effect from the glass substrate.

Concerning the resin preparation, phenyl siloxane polymer resin was prepared with mixing Si-vinyl-functional poly-methyl phenyl siloxane polymers with the Pt catalyst (Part A) and Si-vinyl-functional poly-methyl phenyl siloxane polymers along with the Si-H crosslinker (Part B) at the ratio of (Part A:Part B) 1:3. The curing is carried out by hydrosilylation reaction by introducing these vinyl and SiH functionalities in the presence of the Pt catalyst. An FTIR

* Supplied by Dow Corning Corporation, now Dow Silicones for the experiments reported in this paper. Currently, available from DuPont.

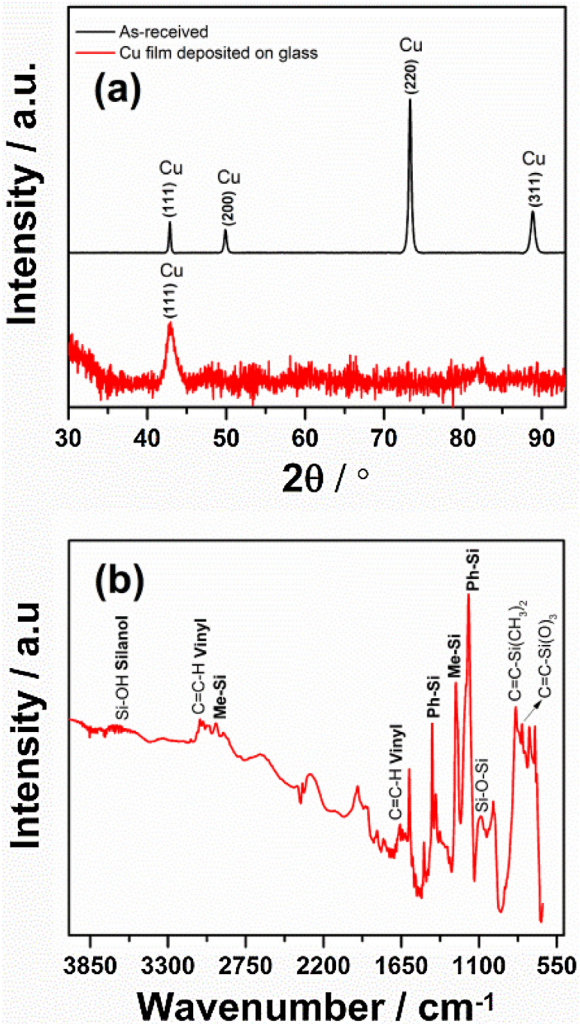

Fig. 1. (a) XRD pattern of substrate and deposited film, (b) FTIR spectrum of silicone coating on copper substrate.

spectrum, recorded on the cured silicone resin coated on the copper alloy substrate, is shown in Fig. 1(b). In the FTIR spectrum, the characteristic out-plane vibration absorption peak of C = C-Si(O)$_3$ was located at 790 cm^{-1}, which can be ascribed to the vinyl-T siloxane resin group. The peak observed at 840 cm^{-1} can be attributed to the vinyl and phenyl-D siloxane resin group [50]. The characteristic symmetric stretching absorption peaks of Si-O-Si bond of linear polysiloxanes appears in the range of 1110 to 990 cm^{-1}. It has been reported that the shape of the broad band appears in this region is presumably due to the formation of chemical bonds between the oxygen atoms of siloxane units and the metal surface [51]. The phenyl groups bonded to the silicon element (Ph-Si) arises at 1183 cm^{-1} and 1434 cm^{-1}, respectively. Analogously, two bands generated by the symmetric deformation vibration and stretching vibration of methyl group attached to the silicon element (Me-Si) were detected at 1265 cm^{-1} and 2960 cm^{-1}. The stretch vibration absorption bands of vinyl group (C = C–H) is located at 3073 cm^{-1} and aromatic C=C bonds arrives at 1662 cm^{-1}. Furthermore, minor addition of silicon hydroxyl was confirmed from the subtle peak located around 3646 cm^{-1}, which is assigned to stretch vibration absorption of Si–OH [50]. Besides the effect of textured growth of copper on impeding the electromigration/dissolution, it is also envisaged that the presence of different organic groups in the silicone encapsulant may have a profound effect on the water and ion transport process.

3.2. Combined EIS and ATR-FTIR studies on Cu film/silicone system

To examine the electrolyte transport kinetics and interfacial chemical changes of the highly textured Cu film/silicone model system concomitantly as a function of exposure time, ATR-FTIR integrated with a potentiostat setup is employed. This integrated configuration enables to probe the transport of water and ionic species and interactions and perturbations of the water uptake through a silicone coating to a Cu film/silicone interface mimicking the water and ion transport pathways encountered in the microelectronic packages. Fig. 2(a, b) shows the EIS spectra of the textured Cu film/silicone model system recorded in a 50 mM NaCl aqueous solution in Nyquist and Bode plot representations, respectively. After 1 h of exposure, a single time constant can be observed from the Nyquist plot (Fig. 2(a)) where a semi-circle arc is observed. Similar behaviour is observed for the silicone coated substrate exposed in chloride environment for the shorter period where diffusion of water and ions seemed to occur inside the coating without any Faradaic reactions [52].

The ATR-FTIR spectra recorded simultaneously during EIS measurements shown in Fig. 3 reveal the sign of stretching or bending vibration bands of water molecules reaching the interface. Within 1 h of immersion, there is no water absorption band observed in the spectra. A broad band appears after 1 h between 3800 to 2900 cm^{-1} with the maxima around 3400 cm^{-1}, implying that water and ions penetrate inside the polymer and this broad band is not only attributed to the symmetric and asymmetric stretching vibration mode ($\nu_{O\text{-}H}$) of water molecules inside the silicone network but also arises from -OH stretching vibration due to copper hydroxide formation at the interface.

The Bode phase angle plot shown in Fig. 2(b) delineates the evolution of relaxation features with their associated characteristic frequencies. The time lag of around 1 h for water and ions to reach the interface was discerned from the single relaxation feature observed in the phase angle plot for 1 h of exposure exhibiting only non-Faradaic reactions [53]. However, one can observe the additional relaxation feature distinctly after 3 h of immersion, revealing Faradaic reactions occur at the interface.

The ATR-FTIR spectra simultaneously obtained reveal that the water stretching bands shift to lower wavenumbers from 3451 to 3378 cm^{-1} with an exposure time shown as inset in Fig. 3(a). This is attributed to different nature of hydrogen bonding interactions within the substrate polymer. The water bands at higher wavenumbers suggest that water molecules first diffuse through free volumes or defects and molecularly disperses with less hydrogen bonding whereas the lower wavenumbers reveal stronger hydrogen bonding between water molecules and the hydrophilic groups of the silicone network [54,55]. This phenomenon is related to the effective dielectric constant of water, ε (shown as schematic in Fig. 3(a)). As the water absorption changes with time, the effective dielectric constant increases as the water molecules bound to the polar groups strongly in the silicone network. Moreover, the H-O-H bending vibration ($\delta_{O\text{-}H}$) of water molecules distinctly appears after 34 h of immersion at lower wavenumber 1620 cm^{-1} (usually appears at 1650 cm^{-1}). The absorbance and the integrated peak area estimated for $\delta_{O\text{-}H}$ is shown in Fig. 3(b). The bending vibration was hard to differentiate effectively in the initial period (< 34 h) as it always overlaps with the polymer bands. However, the appearance of bending vibration at lower wavenumbers ascertains the fact that water molecules form strong hydrogen bonding with the silicone network.

During the initial period of exposure, it is observed from the Bode magnitude plot (Fig. 2(b)) that the magnitude of impedance increases with time in the low frequency range (10 to 0.01 Hz). In principle, impedance at intermediate frequency (10 to 1000 Hz)

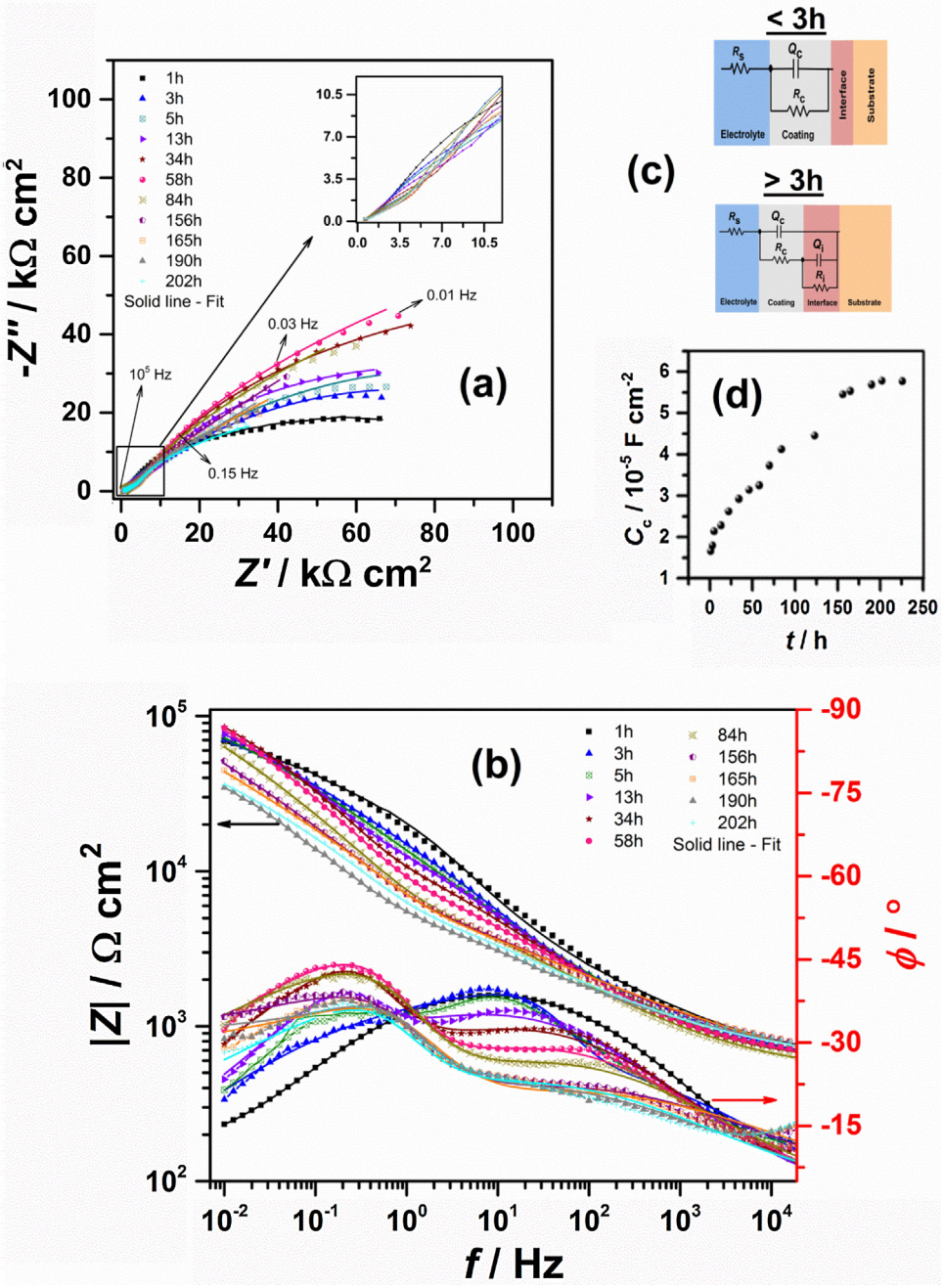

Fig. 2. (a) Nyquist spectra of Cu film/silicone model system recorded in 50 mM NaCl medium at different exposure time. (b) Bode magnitude and phase plot of the developed model system recorded in 50 mM NaCl medium at different exposure time (the solid line is the fit to the experimental data using the equivalent circuit). (c) Equivalent circuits used to model the experimental data. (d) Extracted capacitance values of coating as a function of immersion time.

correspond to coating properties while those at a low frequency contain information related to charge transfer reactions at the coating–metal interface [53]. More specifically, between 3 h and 58 h of immersion, a large increase in the impedance modulus occurs in the low frequency domain whereas the impedance in the intermediate frequency pertinent to the coating diminution. This indicates the formation of corrosion products at the interface which impedes the passage of conducting species to the <111> textured copper surface implying protective surface film formation, thereby enhancing the interfacial charge transfer resistance with time. In principle, the passive film formed on the <111> oriented grains has a more protective Cu_2O layer which alleviates the corrosion kinetics, significantly [56].

In the initial stage (< 3 h), a single bump in the phase angle plot between 1 to 100 Hz is observed indicating the presence of a single time constant [52]. This single relaxation feature is modelled using an equivalent circuit comprising an RC network shown in Fig. 2(c) (< 3 h). The model includes solution resistance R_S, Q_C represents the constant phase element that accounts for non-ideal behavior of the coating capacitance, R_C is the resistance resulting from the formation of ionic conducting paths through the coating. With time, a small narrow bump representing the time constant of coating observed between 10 to 1000 Hz and other denoting the interfacial response evolves at the frequency range between 10 to 0.01 Hz. An equivalent circuit with two RC components shown in Fig. 2(c) (> 3 h) is implemented to fit the experimental data, and

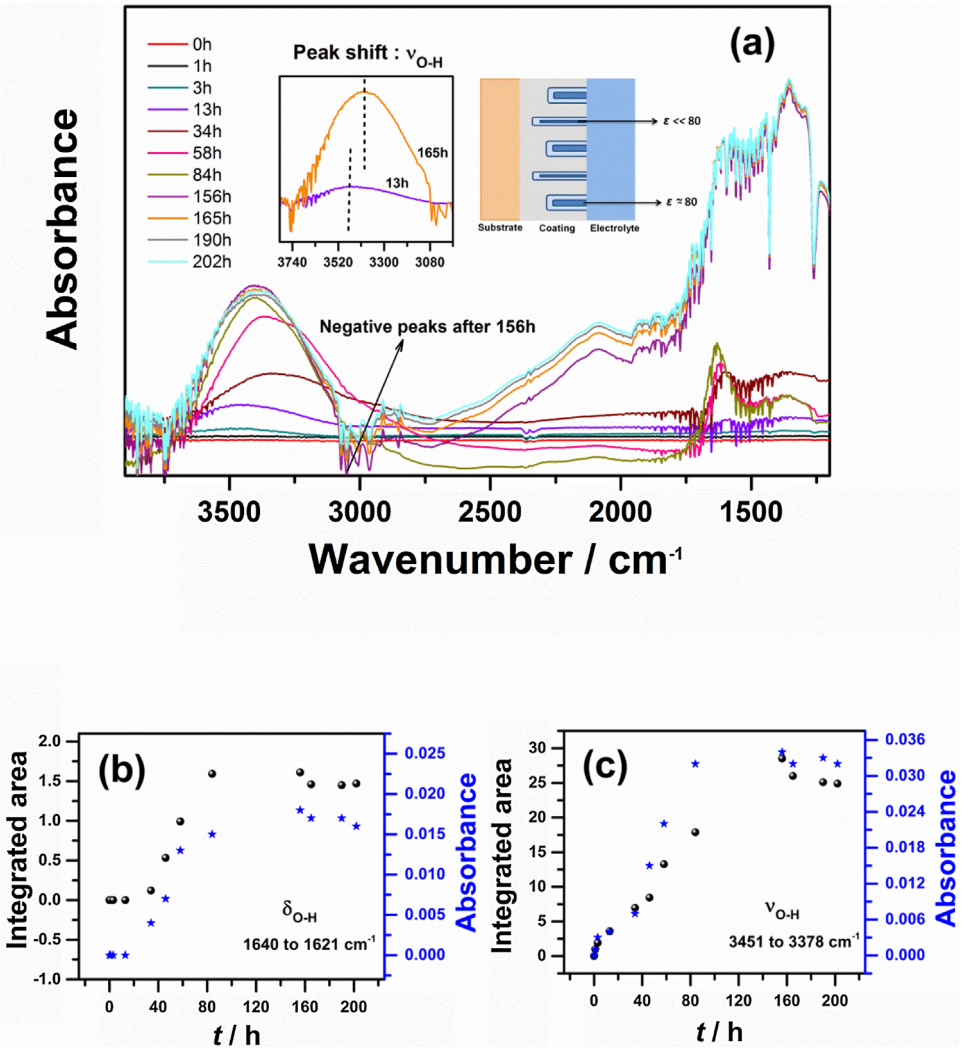

Fig. 3. (a) ATR-FTIR spectra of the Cu film/silicone model recorded simultaneously during EIS measurement in 50 mM NaCl medium at different exposure time. Inset shown is the peak shift observed at different time intervals and schematic presentation of different states of water inside the silicone coating. (b) IR integrated area and absorbance intensities of ν_{O-H} at different exposure time. (c) IR integrated area and absorbance intensities of δ_{O-H} at different exposure timetime.

the Chi square values of less than 10^{-3} was obtained. This circuit includes an additional constant phase element (Q_i) which is parallel to the charge transfer resistance (R_i). It is interesting to see from the Bode phase plots that the appearance of a second relaxation at the low frequency regime varies with the different exposure time. For instance, up to 34 h, the bump in the low frequency region starts to increase from 1 Hz to 0.01 Hz whereas after 58 h the bump starts to emerge from 10 Hz to 0.01 Hz. This implies that the oxide interface starts to rupture locally by the ingress of chloride ions due to the volume expansion of corrosion products. This phenomenon was occurring concurrently with the drop-in impedance at low frequency domain observed from Bode magnitude plot after 58 h of immersion.

However, after 156 h, the impedance modulus at intermediate frequency (10 to 1000 Hz) in the Bode magnitude plot remains constant, indicating the saturation level of water uptake which can be further ascertained from the extracted capacitance (C_C) values from Q_C using Brugg's formula [57] shown in Fig. 2(d). Moreover, the water saturation status can be deciphered from the water absorption bands of ν_{O-H} where the peak area and absorbance levels out, and the values remain constant after 156 h shown in Fig. 3(c). Interestingly, at the same time, negative bands arise after 156 h at around 3072 to 3048 cm^{-1}. In principle, the growth of negative peaks is ascribed to the polymer swelling, delamination or corrosion process at the interface [9]. Due to the smaller depth of penetration at higher wavenumbers [41], the negative peaks in this region corresponds to the corrosion or delamination process occurring at the interface rather than to swelling. The absence of negative peaks at lower wavenumbers implies that there is no alteration of the polymer backbone due to swelling. Consequently, the magnitude of impedance at low frequency drops after 156 h corroborating the present findings indicates that corrosion or delamination is significant at the interface. On the other hand, the effect of chloride ions in destabilizing/degrading the interface could not be monitored from FTIR as it is not IR active. Nevertheless, prior literature confirms that the water uptake is followed by a slow ion uptake and the initiation of a corrosion process at the interface depends on the ionic rather than water arrival [22,23].

3.3. Water transport behaviour in the Cu film/silicone system

A capacitance method is considered to be a reliable method for estimating the water uptake of coating as it has practical relationship with the water permeation of the coating [58]. Based on changes in the coating capacitance, the water absorption and transport characteristics could be evaluated for the developed Cu

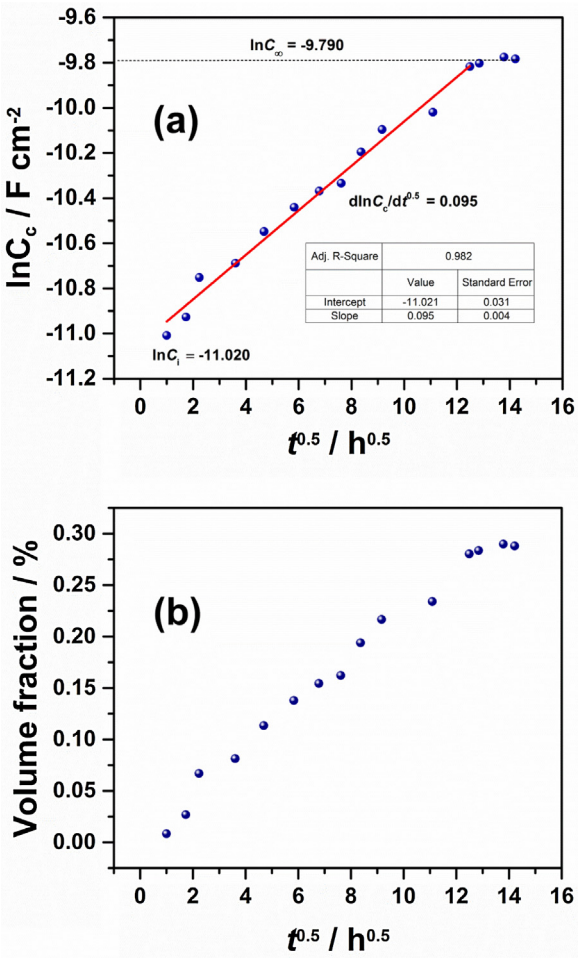

Fig. 4. (a) Time-dependent behaviour of the capacity of the Cu film/silicone model system calculated by the data from the simulated EIS data with the equivalent circuits shown as an inset in Fig. 2(a). (b) Timedependent behaviour of the water uptake of coatings estimated using Eq (3).

film/silicone system. When the electrolyte diffuses into the coating, conduction paths of varying depths form in the coating surface area and the path of water diffusion develops with time (referred to as bulk transport), exhibiting an increase in the capacitance values over time. The linear increase obtained from the ln $C_c \sim t^{1/2}$ curve in Fig. 4(a) indicates that water in the corrosive medium permeated through the micropores and the kinetics observed was a typical Fickian sorption. The water diffusion behaviour in the coating which obeys Fick's law can be calculated from the equation [59] as follows:

$$\frac{\ln C_c - \ln C_i}{\ln C_{sat} - \ln C_i} = \frac{2D^{1/2}}{H\pi^{1/2}} t^{1/2} \quad (1)$$

By deriving the above equation, the following could be obtained:

$$\frac{d\ln C_c}{dt^{1/2}} = \frac{2D^{1/2}}{H\pi^{1/2}} (\ln C_{sat} - \ln C_i) \quad (2)$$

where C_c is the coating capacitance at time t, C_i is the dry coating capacitance at time t =0 h, C_{sat} is the coating capacitance at saturation, and H is the coating thickness. By fitting the linear zone, the intercept of straight line at t =0 h was determined to be -11.020 F cm^{-2} (ln C_i). After 156 h, the coating capacitance showed a plateau region denoting that the water uptake reached saturation, which was the coating capacitance at water saturation (C_{sat}). The calculated diffusion coefficient of water is in the order of 7×10^{-12} m^2 s^{-1}, which is consistent with the diffusivity range of coatings reported in the literature for silicone-based coatings [10,52].

The water absorption volume fraction of the coating i.e. water uptake, ϕ is calculated using the wellknown Brasher and Kingsbury equation assuming that distribution of water occurs randomly at interstitial sites [60],

$$\phi = \frac{\ln C_C/C_i}{\ln (\varepsilon)} \quad (3)$$

where ε (equal to 78.3 at 25 °C) is the dielectric constant of water [60]. The time dependent water absorption volume fraction was in the range of 0% to 0.30% as shown in Fig. 4(b). The values obtained were lower than the range of water absorption volume fraction of silicone-based coatings reported in the literature [52,61]. These results indicated that the silicone coating shows good barrier properties against water penetration into the coatings. Nevertheless, it has been reported that the water uptake kinetics can also be influenced by the ions present in the electrolyte [22]. A detailed discussion on these features is beyond the scope of the current work and will be addressed in the future work. Besides, it is noteworthy that the textured copper film/silicone system using integrated ATR-FTIR and EIS showed that interaction of water with the silicone network at ambient conditions is not only Fickian in nature but also demonstrates the bulk transport pathways of microelectronic packages influencing the water uptake kinetics.

3.4. Interfacial ion transport process and delamination kinetics

The ion transport process along the copper/silicone interface was assessed by monitoring the Volta potential as a function of time in humid atmosphere using SKP measurements. This technique reflects the interfacial transport pathways of corrosive ions and the delamination kinetics occurring beneath the polymer encapsulation in microelectronics and LED packaging systems. The potential profile was measured as point scan over the substrate (Cu alloy), defect edge and intact region (region far away from the defect edge) of the coating at normal (50% RH) and high humidity (93% RH) conditions before adding electrolyte in the defect (figure not shown). Difference in the magnitude of potential at three different locations at both humidity conditions was observed indicating the redistribution of ionic charges with respect to reference probe, accordingly [62]. Remarkably, in the high humid conditions, the potential values shift to more negative values at different locations of the sample (from substrate, defect edge and intact region of coating). After the sample is exposed to the humid air over 20 h, the sample equilibrates with water and the work function difference transforms to less noble potentials (substrate from +800 mV to +300 mV: defect edge: +1000 mV to -1300 mV and intact region: +2500 mV to 150 mV). At high-humid conditions, copper tends to passivate over a period of exposure and the observed potential value of +300 mV is in concordance with the passivation potential of a typical copper electrode [63]. On the other hand, the potential drops significantly to more negative values at the defect and intact region which can be ascribed to the change in the substrate-silicone interfacial chemistry resulting in charge separation in the electrical double layer formed between silicone and the oxidized metal surface [42]. Supposedly, the Si-O- group in the resin interacts with the oxidized copper surface, resulting in the localization of the positive charge in the silicone and negative charge on the copper oxide surface [62]. This scenario induces the oriented dipoles to decrease the electron work function and hence, more negative values are observed at the defect and intact interface. Similar behavior was reported in earlier works with epoxy/alkyd coatings on surface of iron, aluminium, magnesium and zinc decrease the Volta potential by about 200 to 600 mV [62]. In the current system, the Volta potential shifts to even more negative potential by about 1000 mV.

It has been reported that the significant charge transfer interactions result in decrease in work function profoundly, thereby facilitating stronger interfacial bonds [64]. Hence, the very low negative potential observed is attributed to the strong dipole layer interactions between the silicone and the oxidized copper surface.

In order to assess the interfacial stability and delamination kinetics, the effect of exposure time on the spatial potential distribution is monitored by performing a line scan at higher humidity (93%) conditions by adding an aliquot of 50 mM NaCl electrolyte in the defect reservoir. Fig. 5(a) shows the SKP potential profiles recorded as a function of time. After addition of electrolyte with enough ionic strength, the change of Volta potential was observed with exposure time. The scan starts (one hour after addition of electrolyte) from the defect to the intact region after attaining a stable potential at the defect region and the border between defect and the coating is at $X = 0$. The sample description is illustrated in the schematic shown as inset in Fig. 5(a). The galvanic coupling between anodic and cathodic sites is obvious evident from the sharp transition even at early exposure time. This transition evolves with time and is characterized as the delamination front. The time dependence of this potential shift allows us to track the delamination and ion transport kinetics. The potential profiles show that the potential value close to the defect region decreases with increasing the exposure time implying the activation of the metal [46]. Conversely, the strong inhibition of anodic reactions at the intact interface shifts the potential to relatively noble values. Metal dissolution takes place in the defect by releasing electrons which are consumed through oxygen reduction at the delamination front [46]. The hydroxyl ions release at the cathodic sites stimulate the transport of cations (Na^+) from the defect to the delaminating region, generating alkaline sodium hydroxides at the interface. Conceptually, alkaline pH is to be detected at the delamination front and a low pH is to be expected at the defect region and thereby, reflecting the changes in Volta potential with time [47]. The formed alkaline hydroxides change the pH of the interface which destroy the bond between metal oxide and the polymer network. Hence, the nature of formed corrosive species influences the Volta potential. Moreover, mobility of the cations and their ionic concentration

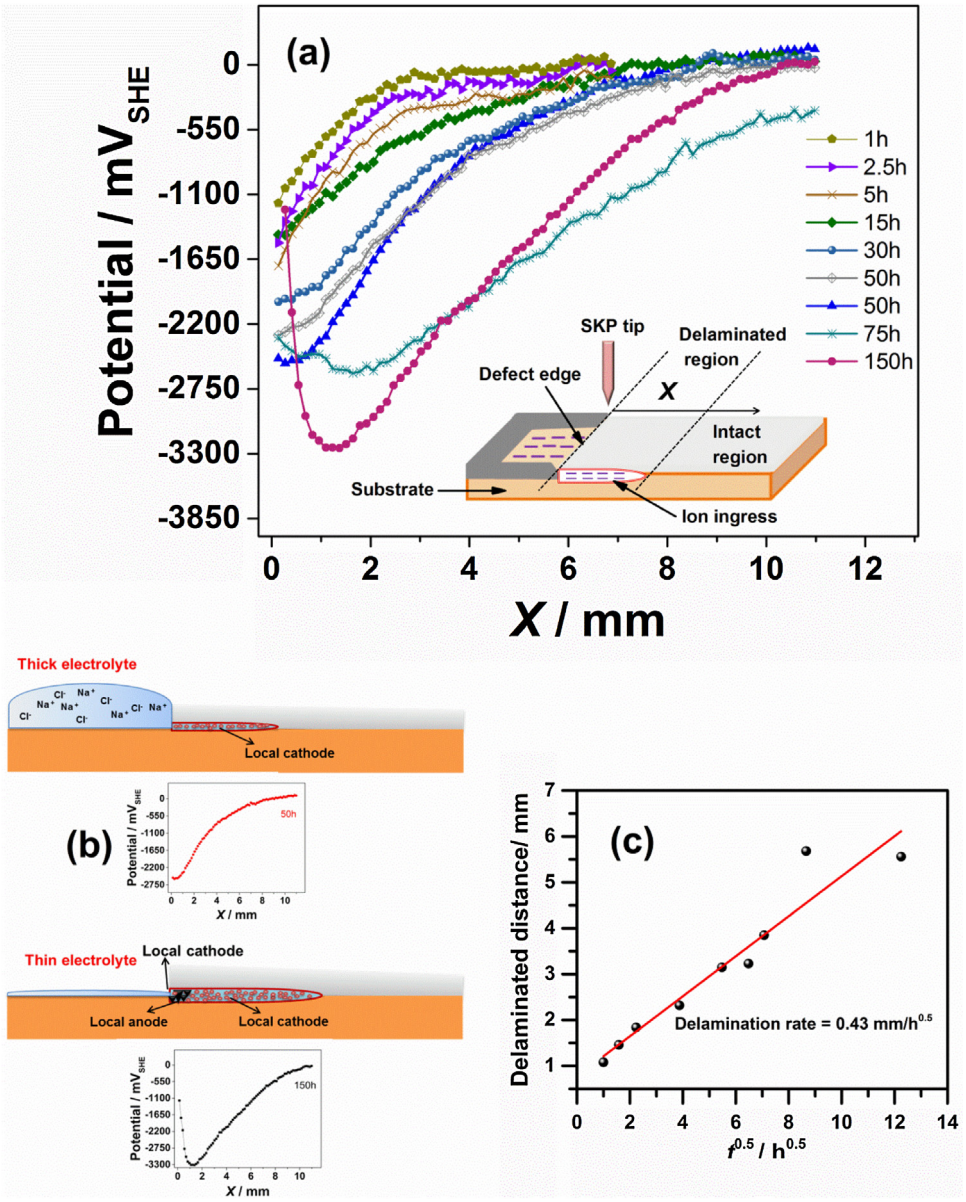

Fig. 5. (a) SKP potential profiles recorded as a function of time in 50 mM defect electrolyte in ambient air of 93% RH. (b) Schematic illustrating change in electrochemical conditions at the interface. (c) A distance of potential displacement for the cathodic front spreading vs square root of time of exposure.

also influences the Volta potential, significantly [47]. Besides, the adsorption of other corrosive species or the intermediate radicals formed or surface intermetallics may modify the Volta potential according to the recent literature on first principle calculations and fundamental studies performed through Kelvin probe measurements on metal surfaces with adsorbed water and corrosive species [65,66].

Over time, the delamination front, which acts as local cathode, proceeds forward with the corrosion products following it. Remarkably, after 75 h to 150 h, the potential starts to decrease towards more negative values observed at the region close to the original defect edge. This discernible shift of potential values towards negative direction implies the existence of local anodes behind the local cathodes (at the defect edge). Moreover, at 150 h, the potential at the defect edge is shifted up and then drops in negative direction more distinctly. Both local galvanic elements exist at the delaminated region as seen from the sharp transition in the potential mapping (shown in Fig. 5(b)). This phenomenon is presumably due to the change in electrochemical conditions at the interface. After 75 h of exposure in humid conditions, the electrolyte thickness reduces at the defect area. This situation assuages the supply of oxygen and Na^+ ions from the metal surface to the interface, however the delamination front proceeds forward at the local cathode (delaminated interface). At prolonged time of exposure, corrosion product near the coating defect edge can be formed trailing a local anode which will be positioned between two cathodic areas: the corrosion product area near the coating defect edge trailing it and the cathodic delaminated area preceding it, as shown in the Volta potential scan after 150 h of exposure. The corrosion is then confined to one location where the small anodic area shows a high oxidation rate which is reflected by the sharp drop of the potential in the negative direction close to the defect edge embedded between the higher Volta potential values at the coating defect edge, at which the corrosion products are formed, and those at the delaminated area. Hence, the formation of corrosion products plays a strong role in changing the potential values. Similar behaviour was observed in the literature due to the change of oxygen activity [47].

However, the anodic area does not progress significantly even with longer exposure time implying that only local corrosion takes place at the defect boundary. As the progress rate of the anodic front is insignificant with time, only the cathodic delamination front position was plotted as a function of square root of time (Fig. 5(c)) using the procedure followed in the literature reports [67]. The estimated average delamination rate is 0.43 mm $h^{-1/2}$.

Earlier reports [68,69] on the mixed mode of delamination proved that depending on the electrochemical conditions of the metal surface the mode of delamination can switch. McCafferty [68] demonstrated that in the bulk electrolyte, the current distribution is more uniform whereas in the thin electrolyte conditions, a geometry effect must be considered and hence the current flow is concentrated near the anode/cathode juncture. This circumstance

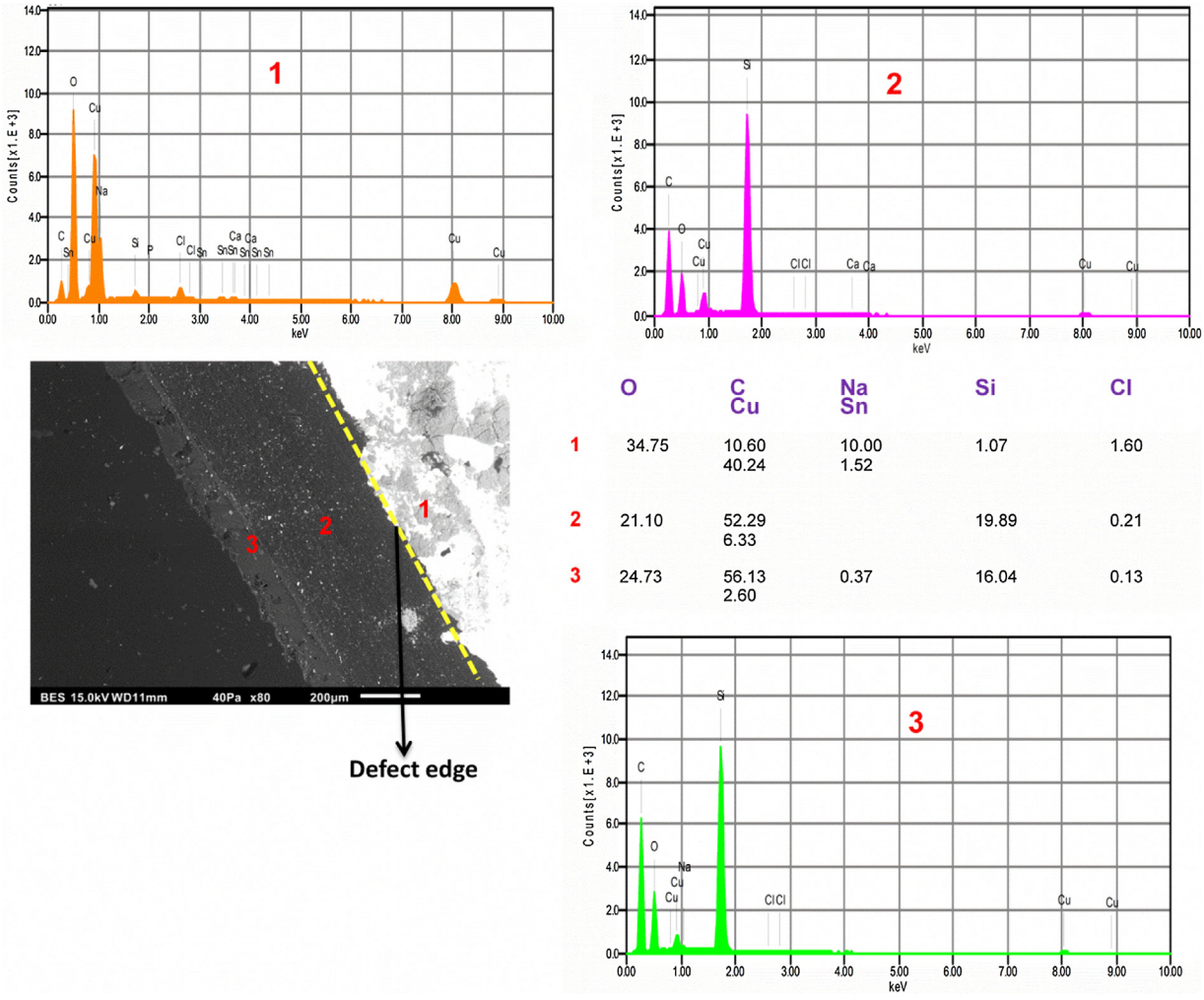

	O	C Cu	Na Sn	Si	Cl
1	34.75	10.60 40.24	10.00 1.52	1.07	1.60
2	21.10	52.29 6.33		19.89	0.21
3	24.73	56.13 2.60	0.37	16.04	0.13

Fig. 6. SEM micrograph and EDX spectra of sample collected after SKP measurement.

alters the shape and dimension of the delamination front for both modes. Conceptually, very high anodic currents will be generated at the boundary where the anodic dissolution of copper is predominant to compensate the oxygen reduction reactions.

Important observations were made by El Warraky *et al.* [70] in chloride containing solutions showing that the pitting corrosion occurs on the copper surface at a concentration higher than 10^{-2} M, which is similar to the concentration range used in the present work. It was confirmed that the chloride ions act in the formation of cuprous oxide and they were responsible for the localized attack. Moreover, Pan *et al.* [71] demonstrated that double-layered corrosion product was formed in chloride solutions comprising inner cuprous oxide and outer layer composed of more chloride. Accordingly, it is observed from the EDX spectra as a point scan from SEM studies (Fig. 6) that the chloride ions concentrated underneath the coating close to the defect edge, corroborating our present findings of existence of a local anode in front of a local cathode. On the other hand, sodium was found in the areas at the delaminated interface (point scan 3) and no significant enrichment of sodium at the defect boundary (point scan 2). As such, the switching of delamination mode is attributed to the change in electrochemical conditions with time and the interfacial transport of cations control the cathodic delamination propagation kinetics.

4. Conclusions

The water and ion transport process occurring along the two different conducting pathways (bulk and interfacial transport) of developed copper/silicone model system was investigated using integrated *in-situ*ATR-FTIR with EIS analysis and SKP technique. The principal findings of this work is as follows,

(1) Integrated *in-situ* ATR-FTIR and EIS studies on textured Cu film/silicone model system concomitantly proved that water uptake of the polymer increases with time and saturates over a certain period. The different nature of hydrogen bonding interactions and the water saturation status was deciphered from the variation in water absorption bands with time. The distinct detection of an additional time constant in the impedance spectra emerging over time is attributed to the changes in the interfacial (electro)chemistry.
(2) Using the coating capacitance values estimated at different time intervals, the textured copper film/silicone system showed that diffusion of water within the silicone network at ambient conditions is Fickian in nature. The estimated diffusion coefficient of water in chloride environment was in the order of 7×10^{-12} m^2s^{-1} and the obtained water absorption volume fraction was in the range of 0% to 0.3%, offering significant barrier performance and corrosion protective properties.
(3) SKP measurements revealed that the oriented dipoles formed between the oxide surface and the silicone coating shifted the Volta potential in the negative direction. The observed mixed mode of delamination is attributed to the evolution of local anodes at the interface yet the interfacial transport of cation controls the cathodic delamination propagation kinetics.

Acknowledgements

This work was financially supported by NWO-TTW, The Netherlands (project no.13893). The authors would like to thank Amar Mavinkurve and Michiel van Soestbergen from NXP semiconductors for their valuable suggestion. Also, the authors would like to thank Dow Silicones Belgium for the supply of the silicone resins.

References

[1] Y. Zeng, K. Bai, H. Jin, Microelectron. Reliab. 53 (2013) 985–1001.
[2] S. Wagner, K. Höppner, M. Töpper, O. Wittler, K.D. Lang, PCIM Eur. Conf. Proc., 2014, pp. 1078–1084.
[3] L. Lantz, M.G. Pecht, IEEE Trans. Components Packag. Technol. 26 (2003) 199–205.
[4] M.S. Jellesen, D. Minzari, U. Rathinavelu, P. Møller, R. Ambat, ECS Trans. 25 (30) (2010) 1–14.
[5] M. Van Soestbergen, A. Mavinkurve, R.T.H. Rongen, K.M.B. Jansen, L.J. Ernst, G.Q. Zhang, Electrochim. Acta 55 (2010) 5459–5469.
[6] O.V. Elisseeva, A. Bruhn, J. Cerezo, A. Mavinkurve, R.T.H. Rongen, G.M. O'Halloran, R. Ambat, H. Terryn, J.M.C. Mol, Corros. Eng. Sci. Technol. 48 (2013) 409–417.
[7] A. Herrmann, S.J.F. Erich, L.G.J.V.D. Ven, W.D.V. Driel, M. van Soestbergen, A. Mavinkurve, F.D. Buyl, O.C.G. Adan, 18th Int. Conf. Therm. Mech. Multi-Physics Simul. Exp. Microelectron. Microsystems, 2017, pp. 1–6.
[8] V.N. Nguyen, F.X. Perrin, J.L. Vernet, Corros. Sci. 47 (2005) 397–412.
[9] M. Öhman, D. Persson, Electrochim. Acta 52 (2007) 5159–5171.
[10] X. Yuan, Z.F. Yue, X. Chen, S.F. Wen, L. Li, Prog. Org. Coat 78 (2015) 168–175.
[11] O.A. Stafford, B.R. Hinderliter, S.G. Croll, Electrochim. Acta 52 (2006) 1339–1348.
[12] S. Pandiyan, J. Krajniak, G. Samaey, D. Roose, E. Nies, Comput. Mater. Sci. 106 (2015) 29–37.
[13] V.B. Mišković-stanković, D.M. Dražić, M.J. Teodorović, Corros. Sci. 37 (1995) 241–252.
[14] Y. Dong, Q. Zhou, Corros. Sci. 78 (2014) 22–28.
[15] M.D. Grosso Destreri, J. Vogelsang, L. Fedrizzi, Prog. Org. Coat 37 (2002) 57–67.
[16] A.S. Castela, A.M. Simões, Prog. Org. Coat. 46 (2003) 130–134.
[17] V.N. Nguyen, F.X. Perrin, J.L. Vernet, Corros. Sci. 47 (2005) 397–412.
[18] N. Fredj, S. Cohendoz, S. Mallarino, X. Feaugas, S. Touzain, Prog. Org. Coati. 67 (2010) 287–295.
[19] F. Mansfeld, H. Xiao, L.T. Han, C.C. Lee, Prog. Org. Coat 30 (1997) 89–100.
[20] B. Normand, H. Takenouti, M. Keddam, H. Liao, G. Monteil, C. Coddet, Electrochim. Acta 49 (2004) 2981–2986.
[21] R.G. Duarte, A.S. Castela, M.G.S. Ferreira, Prog. Org. Coat. 65 (2009) 197–205.
[22] M. Dornbusch, S. Kirsch, C. Henzel, C. Deschamps, S. Overmeyer, K. Cox, M. Wiedow, U. Tromsdorf, M. Dargatz, U. Meisenburg, Prog. Org. Coat. 89 (2015) 332–343.
[23] F. Bellucci, J. Electrochem. Soc. 138 (2006) 40–48.
[24] M.M. Madani, R.R. Kodnani, R.D. Granata, IEEE Trans. Reliab. 46 (1997) 45–51, 55.
[25] J. Lumsden, J. Kuo, G. Pollock, Components Technol. Conf. (2002) 219–224.
[26] R. Vlasak, I. Klueppel, G. Grundmeier, Electrochim. Acta 52 (2007) 8075–8080.
[27] M. Öhman, D. Persson, C. Leygraf, Solid-State Lett. 10 (2007) C27.
[28] P. Taheri, J.H.W. de Wit, H. Terryn, J.M.C. Mol, J. Phys. Chem. C 117 (2013) 20826–20832.
[29] P. Taheri, M. Ghaffari, J.R. Flores, F. Hannour, J.H.W. De Wit, J.M.C. Mol, H. Terryn, J. Phys. Chem. C 117 (2013) 2780–2792.
[30] M. Sababi, H. Terryn, J.M.C. Mol, Prog. Org. Coat. 105 (2017) 29–36.
[31] K. Ho, A. Teng, Survey on Delamination of IC Packages in Electronic Products, in: Int. Symp. Electron. Mater. Packag. (Cat. No.00EX458), IEEE, 2000, pp. 269–273.
[32] W. Wang, K. Pan, T. Li, X. Han, W. Cao, S. Gong, W. Wang, K. Fan, 18th Int. Conf. Electron. Packag. Technol., IEEE, 2017, pp. 1542–1546.
[33] B. Hamon, W.D.V. Driel, Microelectron. Reliab. 64 (2016) 599–604.
[34] W.J.L. Suyker, M.P. Buijsrogge, P.T.W. Suyker, C.W.J. Verlaan, C. Borst, P.F. Gründeman, J. Thorac. Cardiovasc. Surg. 127 (2004) 498–503.
[35] Y. Shuto, H. Sato, M. Fukuda, S. Tohno, Commun. Japan, Part II Electron. (English Transl. Denshi Tsushin Gakkai Ronbunshi) 81 (1998) 17–26.
[36] M. Itoh, M. Suto, T. Iimura, J.H. Chae, R.G. Schmidt, RadTech Asia Proc. 1–3 (2016) 24–27.
[37] S. Wang, X. Chen, X. Liu, F. Chen, B. Cao, S. Liu, IEEE3th Int. Conf. Electron. Packag. Technol. High Density Packag2012, 3th Int. Conf. Electron. Packag. Technol. High Density Packag (2012) 1451–1454.
[38] S.D.L. Zhong, S.H.Y. Zou, J.C.C. Lo, S.W.R. Lee, IEEE14th Int. Conf. Electron. Packag. Technol.2013, 14th Int. Conf. Electron. Packag. Technol. (2013) 612–616.
[39] K. Suzuki, T. Higashino, K. Tsubosaki, A. Kabashima, K. Mine, K. Nakayoshi, IEEE Trans. Components, Hybrids, Manuf. Technol. 13 (1990) 883–887.
[40] A. Leng, H. Streckel, M. Stratmann, Corros. Sci. 41 (1998) 547–578.
[41] K. Wapner, M. Stratmann, G. Grundmeier, Electrochim. Acta 51 (2006) 3303–3315.
[42] J. Wielant, R. Posner, G. Grundmeier, H. Terryn, J. Phys. Chem. C 112 (2008) 12951–12957.
[43] M. Rohwerder, S. Isik-Uppenkamp, C.A. Amarnath, Electrochim. Acta 56 (2011) 1889–1893.
[44] M. Santa, R. Posner, G. Grundmeier, J. Electrochem. Soc. 158 (2011) C36.
[45] A. Nazarov, A.P. Romano, M. Fedel, F. Deflorian, D. Thierry, M.G. Olivier, Corros. Sci. 65 (2012) 187–198.
[46] A. Leng, H. Streckel, M. Stratmann, Corros. Sci. 41 (1998) 547–578.
[47] A. Leng, H. Streckel, M. Stratmann, Corros. Sci. 41 (1998) 579–597.
[48] G.L. Song, R. Mishra, Z. Xu, Electrochem. Commun. 12 (2010) 1009–1012.
[49] T. Hara, H. Toida, Y. Shimura, Electrochem. Solid-State Lett. 6 (2003) G98–G100.

[50] A.L. Smith, The Analytical Chemistry of Silicones, Wiley, New York, 1991.
[51] R.F. Willis, Tribology 2 (1969) 175–178.
[52] X. Yuan, Z.F. Yue, X. Chen, S.F. Wen, L. Li, T. Feng, Prog. Org. Coat 86 (2015) 41–48.
[53] T. Feng, S.F. Wen, X. Yuan, Z.Q. Liu, Z.F. Yue, L. Li, J. Coatings Technol. Res. 13 (2015) 123–132.
[54] P. Sutandar, D.J. Ahn, E.I. Franses, Macromolecules 27 (1994) 7316–7328.
[55] M. Liu, P. Wu, Y. Ding, S. Li, Phys. Chem. Chem. Phys. 5 (2003) 1848–1852.
[56] E. Martinez-Lombardia, Y. Gonzalez-Garcia, L. Lapeire, I. De Graeve, K. Verbeken, L. Kestens, J.M.C. Mol, H. Terryn, Electrochim. Acta 116 (2014) 89–96.
[57] G.J. Brug, A.L.G. van den Eeden, M. Sluyters-Rehbach, J.H. Sluyters, J. Electroanal. Chem. 176 (1984) 275–295.
[58] E.P.M. van Westing, G.M. Ferrari, J.H.W. de Wit, Corros. Sci. 36 (1994) 957–977.
[59] D.Y. Perera, P. Selier, Prog. Org. Coat 2 (1973) 57–80.
[60] D.M. Brasher, A.H. Kingsbury, J. Appl. Chem. 4 (2007) 62–72.
[61] X. Yuan, Z.F. Yue, X. Chen, S.F. Wen, L. Li, Prog. Org. Coat. 78 (2015) 168–175.
[62] A.P. Nazarov, D. Thierry, Electrochim. Acta 49 (2004) 2955–2964.
[63] H.H. Strehblow, B. Titze, Electrochim. Acta 25 (1980) 839–850.
[64] J. Wielant, R. Posner, R. Hausbrand, G. Grundmeier, H. Terryn, Surf. Interface Anal. 42 (2010) 1005–1009.
[65] C. Örnek, M. Liu, J. Pan, Y. Jin, C. Leygraf, Top. Catal. 61 (2018) 1169–1182.
[66] C. Örnek, C. Leygraf, J. Pan, Corros. Eng. Sci. Technol. 54 (2019) 185–198.
[67] A. Leng, H. Streckel, K. Hofmann, M. Stratmann, Corros. Sci. 41 (1998) 599–620.
[68] E. McCafferty, J. Electrochem. Soc. 124 (2006) 1869.
[69] A. Nazarov, D. Thierry, Corrosion 66 (2010) 0250041–02500410.
[70] A. El Warraky, H.A. El Shayeb, E.M. Sherif, Anti-Corros. Methods Mater. 51 (2004) 52–61.
[71] C. Pan, W. Lv, Z. Wang, W. Su, C. Wang, S. Liu, J. Mater. Sci. Technol. 33 (2017) 587–595.